



Article

Geometrical Analysis of an Oscillating Water Column Converter Device Considering Realistic Irregular Wave Generation with Bathymetry

Ana Paula Giussani Mocellin ^{1,2}, Rafael Pereira Maciel ², Phelype Haron Oleinik ²,
Elizaldo Domingues dos Santos ², Luiz Alberto Oliveira Rocha ², Juliana Sartori Ziebell ¹,
Liércio André Isoldi ^{2,*} and Bianca Neves Machado ³

- ¹ Institute of Mathematics and Statistics, Federal University of Rio Grande do Sul (UFRGS), Porto Alegre 91509-900, RS, Brazil; ana.mocellin@ufrgs.br (A.P.G.M.); julianaziebell@ufrgs.br (J.S.Z.)
² School of Engineering, Federal University of Rio Grande (FURG), Rio Grande 96203-900, RS, Brazil; rafaelmaciel95@hotmail.com (R.P.M.); phe.h.o1@gmail.com (P.H.O.); elizaldosantos@furg.br (E.D.d.S.); luizrocha@furg.br (L.A.O.R.)
³ Interdisciplinary Department, Federal University of Rio Grande do Sul (UFRGS), Tramandaí 95590-000, RS, Brazil; bianca.machado@ufrgs.br
* Correspondence: liercioisoldi@furg.br; Tel.: +55-53-99109-7356

Abstract: Given the increasing global energy demand, the present study aimed to analyze the influence of bathymetry on the generation and propagation of realistic irregular waves and to geometrically optimize a wave energy converter (WEC) device of the oscillating water column (OWC) type. In essence, the OWC WEC can be defined as a partially submerged structure that is open to the sea below the free water surface (hydropneumatic chamber) and connected to a duct that is open to the atmosphere (in which the turbine is installed); its operational principle is based on the compression and decompression of air inside the hydropneumatic chamber due to incident waves, which causes an alternating air flow that drives the turbine and enables electricity generation. The computational fluid dynamics software package Fluent was used to numerically reproduce the OWC WEC according to its operational principles, with a simplification that allowed its available power to be determined, i.e., without considering the turbine. The volume of fluid (VOF) multiphase model was employed to treat the interface between the phases. The WaveMIMO methodology was used to generate realistic irregular waves mimicking those that occur on the coast of Tramandaí, Rio Grande do Sul, Brazil. The constructal design method, along with an exhaustive search technique, was employed. The degree of freedom H_1/L (the ratio between the height and length of the hydropneumatic chamber of the OWC) was varied to maximize the available power in the device. The results showed that realistic irregular waves were adequately generated within both wave channels, with and without bathymetry, and that wave propagation in both computational domains was not significantly influenced by the wave channel bathymetry. Regarding the geometric evaluation, the optimal geometry found, $(H_1/L)_0 = 0.1985$, which maximized the available hydropneumatic power, i.e., the one that yielded a power of 25.44 W, was 2.28 times more efficient than the worst case found, which had $H_1/L = 2.2789$.

Keywords: irregular waves; OWC device; WaveMIMO methodology



Citation: Mocellin, A.P.G.; Maciel, R.P.; Oleinik, P.H.; dos Santos, E.D.; Rocha, L.A.O.; Ziebell, J.S.; Isoldi, L.A.; Machado, B.N. Geometrical Analysis of an Oscillating Water Column Converter Device Considering Realistic Irregular Wave Generation with Bathymetry. *J. Exp. Theor. Anal.* **2023**, *1*, 24–43.
<https://doi.org/10.3390/jeta1010003>

Academic Editor: Marco Rossi

Received: 1 August 2023

Revised: 7 September 2023

Accepted: 11 September 2023

Published: 19 September 2023



Copyright: © 2023 by the authors. Licensee MDPI, Basel, Switzerland. This article is an open access article distributed under the terms and conditions of the Creative Commons Attribution (CC BY) license (<https://creativecommons.org/licenses/by/4.0/>).

1. Introduction

As technological and scientific advances in human society progress, we are faced with an increase in the global energy demand that is a consequence of socio-economic development and the improvement in the population's quality of life [1]. Since around 1850, fossil fuels such as coal, oil, and gas have dominated the energy supply, which has led to a significant increase in greenhouse gas emissions. As a result, the consumption of these non-renewable energy sources is responsible for most of the global anthropogenic emissions of these gases [2].

Since the turn of the century, due to the increase in investments in the renewable energy market, technological advances, and higher development rates in countries, the energy sector has undergone a major change [3]. As a consequence, there has been accelerated development of non-conventional energy sources and technological advances in the exploitation of all forms of energy. This fact has helped to reduce prices, decoupling the concept of economic growth from the emission of gases that cause the greenhouse effect. Therefore, most countries have sought to diversify their energy matrix [1,3].

Among the renewable energy sources, it is possible to highlight the energy that comes from the oceans. The ocean can be considered a great reservoir of thermal and mechanical energy [4]. However, due to the low quality of heat and the high entropy within the marine environment, as well as the current level of technological advances, only mechanical energy can be used effectively. Ocean energy can be subdivided by origin into tides, waves, marine currents, temperature gradients, and salinity [5].

Wave energy is a concentrated form of solar energy: the sun produces temperature differences, causing winds to blow over the ocean surface. The waves generated are capable of traveling thousands of kilometers with almost no energy loss [6]. In Southern Brazil, the theoretical energy potential that can be obtained from ocean waves is 35 GW, which is higher than the potential found in other regions of the country [4].

The conversion of energy contained in ocean waves into electrical energy is carried out by means of devices such as an oscillating water column (OWC), which consists of a partially submerged hollow concrete structure. The OWC is composed of a hydropneumatic chamber and a duct, in which a turbine and an electric generator are coupled. The device chamber is open below the free water surface and the duct is open to the atmosphere; thus, the incidence of waves on the device makes the water column inside the chamber oscillate and generate a local pressure, expelling or sucking air through the duct. Consequently, this air flow drives the turbine, activating an electric generator [7].

Due to current and future needs in terms of using renewable energy sources, as well as the energy potential of the Brazilian coast, knowledge of how sea wave energy can be converted into electrical energy is essential, so that this type of technology can be used fully and sustainably. One of the methods to develop knowledge is through numerical simulation, which is a tool to study wave energy converter (WEC) devices, which in turn allows the construction of these devices (after testing), with the overall aim of their use in an optimized way with regard to energy conversion [8,9]. Regarding computational modeling as applied to OWC WEC devices, most studies approach regular waves (such as [10–12]). However, some recent research has been developed considering the incidence of irregular waves on OWC converters (such as [13–15]).

There are also other ways to study the hydrodynamic behavior of WEC devices. Mavrakos et al. [16] addressed the hydrodynamics of bottomless cylindrical bodies with a vertical axis of symmetry floating in finite-depth water using two methods: an analytical approach and a CFD method. In this case, moonpool-type floaters were used, which have been employed as OWC-type devices. In turn, Zabala et al. [17] proposed experimental wave tank tests to validate a numerical model of wave tanks based on CFD that allowed, with limited resources, the necessary simulations for the design and optimization of marine WEC devices under various sea state conditions.

To maximize energy conversion, several studies have applied the constructal design method in the geometric evaluation of WEC devices [18–21]. Constructal design allows the device geometry to be subjected to global constraints and varied according to degrees of freedom [22]. To apply it, it is necessary to determine the performance indicator, the degrees of freedom, and geometric restrictions. The restrictions used in the present study were the volume of the hydropneumatic chamber and the total volume of the device; both were kept constant. The evaluated degree of freedom was the ratio between the height and the length of the hydropneumatic chamber. Finally, the performance indicator used was the OWC's available power.

Therefore, the present study aims to develop an investigation regarding the influence (on the numerical wave generation and propagation) of the bathymetry of the municipality of Tramandaí, Brazil. Then, we analyzed and performed the geometric optimization of an OWC WEC device, through the constructal design method associated with an exhaustive search technique, while employing realistic irregular waves representing a sea state that occurred on 28 May 2018, at 10:14 a.m. For this purpose, numerical simulations were conducted considering two-dimensional computational modeling of the OWC WEC device.

2. Materials and Methods

The advancement of WECs is defined by the diversity of ideas and concepts on how to use resources from wave energy [23]. Therefore, WEC devices can be classified according to different criteria, such as the distance from the coast (onshore, nearshore, and offshore) or their conversion principle (OWC, oscillating bodies, and overtopping devices). Among these WECs, this study considered the OWC, as previously done in similar studies [24–26], which, as mentioned, is a partially submerged hollow structure, open to the sea below the free water surface. With the passage of the waves, there is an elevation and descent of the water column inside the chamber, which displaces the air through a turbine, thus generating electrical energy. Figure 1 illustrates this principle.

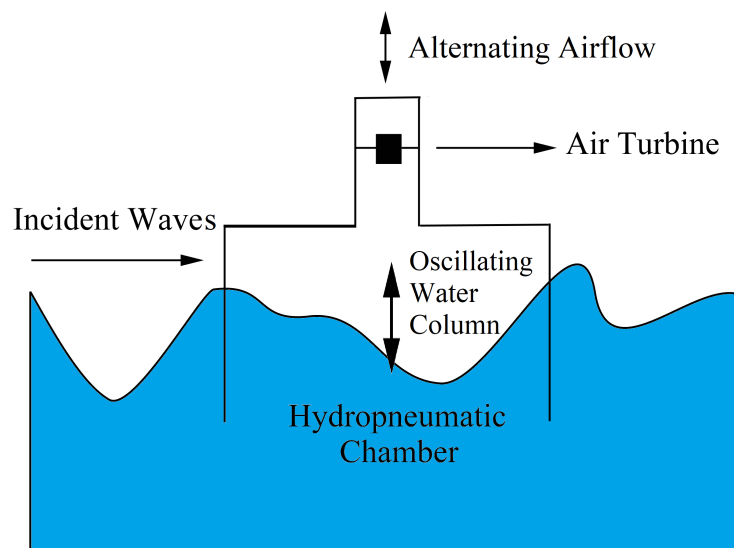


Figure 1. Physical operating principle of an OWC device.

Models that describe the wave behavior and their incidence on an OWC WEC can be classified based on theories of regular and irregular waves. Regular wave theories allow waves with well-defined and constant behavior in each period of time or space, whereas, in irregular wave theories, waves are created from the sum of small regular waves with different heights and periods. Among the existing models, those that employ irregular waves are the ones that best represent realistic sea state conditions in oceanic environments [8]. Therefore, in this study, only realistic irregular waves were simulated. However, the characteristics of representative regular waves were used to discretize the computational model. For this reason, the characteristics of regular waves are shown in Figure 2.

In Figure 2, h is the water depth (m), H is the wave height (m), A is the wave amplitude (m), λ is the wavelength, MWL is the mean water level, and η is the free surface elevation (m). Another important characteristic is the wave period (T , in s), which represents the time required for two successive crests (or two successive troughs) to reach a specific point [27].

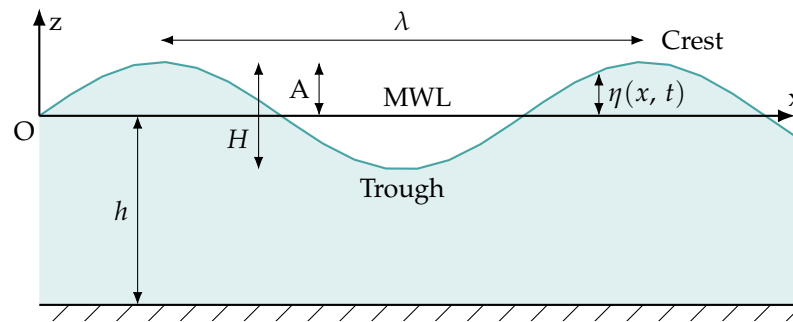


Figure 2. Regular waves characteristics.

2.1. Mathematical and Numerical Modeling

In this study, the computational fluid dynamics (CFD) software package Fluent was employed for the numerical simulations regarding the operating principle of the OWC WEC. Fluent is a computational program, based on the finite volume method (FVM), which allows the numerical simulation of fluid flow and heat transfer in complex geometries [28].

The volume of fluid (VOF) multiphase model, proposed by Hirt and Nichols [29], was used to treat the interface between the fluids. This model employs the technique of representing the phases (air and water) inside each computational cell as a volumetric fraction (α), in which the sum of the phases in each cell is unitary; therefore, $\alpha_{water} + \alpha_{air} = 1$.

In the VOF model, only one set of equations is used, consisting of the conservation equations for mass, volume fraction, and momentum [30]:

$$\frac{\partial \rho}{\partial t} + \nabla \cdot (\rho \vec{v}) = 0 \tag{1}$$

$$\frac{\partial \alpha}{\partial t} + \nabla \cdot (\alpha \vec{v}) = 0 \tag{2}$$

$$\rho \frac{\partial \vec{v}}{\partial t} + \rho (\nabla \cdot \vec{v}) \vec{v} = -\nabla p + \nabla \cdot \bar{\bar{\tau}} - \rho \vec{g} + S \tag{3}$$

where ρ is the density (kg/m^3), t is the time (s), \vec{v} is the velocity vector (m/s), p is the static pressure (Pa), $\bar{\bar{\tau}}$ is the strain rate tensor (N/m^2), \vec{g} is the gravity acceleration (m/s^2), and S is the source term representing the energy dissipation when a numerical beach is implemented (N/m^3).

It is worth mentioning that the continuity and momentum equations are solved for the mixture, therefore, the density (ρ) and viscosity (μ) of the mixture can be described respectively, by [31]:

$$\rho = \alpha_{water} \rho_{water} + \alpha_{air} \rho_{air} \tag{4}$$

$$\mu = \alpha_{water} \mu_{water} + \alpha_{air} \mu_{air} \tag{5}$$

Lastly, some numerical parameters were adopted to control the solution of the numerical simulations. The first-order upwind was used for the discretization of the momentum equation, assuming that the value of the variable in the center of the control volume could be considered as the average value of the entire volume; the PRESTO (PResure STaggering Option) was used for pressure discretization; the geo-reconstruct scheme was employed to tackle the volumetric fraction; and PISO (Pressure-Implicit Splitting of Operators) was used for the pressure–velocity coupling, based on the highest degree of approximation between the corrections for pressure and velocity. The algorithm presented two additional correlations, neighbor correction and skewness correction, which increased the calculation efficiency. This numerical computational model has already been used in previous works (see [21,32]).

2.2. WaveMIMO Methodology

Machado et al. [33] proposed a numerical technique for the simulation of irregular waves, which may represent a realistic sea state in a given region; they named this technique the WaveMIMO methodology, which has been verified and validated for regular wave generation in Maciel et al. [34]. For this, in the present study, a wave spectrum was obtained from the spectral model TOMAWAC (Telemac-based Operational Model Addressing Wave Action Computation). This spectrum was transformed into a time series of free surface elevations and then transformed into orbital velocity profiles. With this, the discrete data obtained could be imposed as boundary conditions of wave velocity in a wave channel in the Fluent software, thus enabling the numerical simulation of realistic irregular waves. In summary, the WaveMIMO methodology was applied in the present work by means of the following steps.

- Location and time of study: a place and a time interval were chosen, and, thus, a simulation of the sea state was performed with these conditions.
- TOMAWAC: the software was used for the numerical simulation of the sea state.
- Wave spectrum simulation: a wave spectrum was extracted from the sea state simulation at the chosen location and time interval.
- Spectral data conversion: the wave spectrum was transformed into a free surface elevation time series statistically identical to the initial wave spectrum, thus representing the sea state [33].
- Dispersion relation: η was decomposed into horizontal (u) and vertical (w) velocity components using the method presented by Machado et al. [33] and Oleinik et al. [35].
- Orbital velocities u and w : velocity profiles were imposed as boundary conditions in Fluent to generate a realistic sea state.

For the present work, a sea state that occurred in Tramandaí, in the state of Rio Grande do Sul, Brazil, was considered. This sea state condition happened on 28 May 2018, at 10:14 am, at a study area located 2094.33 m from the coast, with geographic coordinates $50^{\circ}06'18''$ W and $29^{\circ}59'52''$ S (see Figure 3).

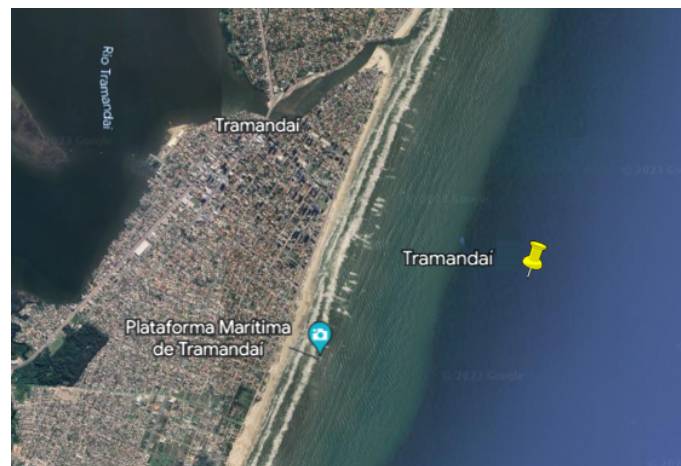


Figure 3. Location of the study area.

In order to determine the most frequent sea state, realistic data of the significant height (H_s) and mean period (T_m) referring to the selected study area were analyzed. For this, a wave recurrence bivariate histogram relating T_m and H_s was designed, which can be seen in Figure 4.

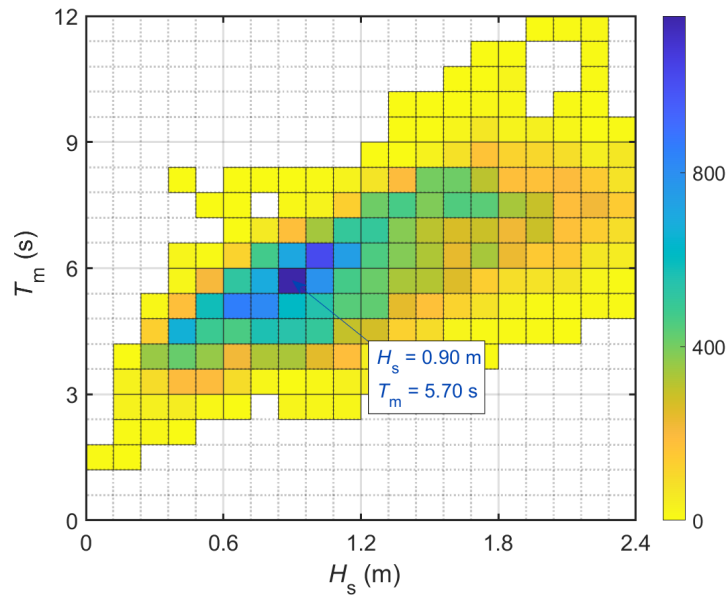


Figure 4. Bivariate histogram of H_s and T_m .

Next, the wavelength (λ) was calculated using the dispersion relation equation [27]:

$$\sigma^2 = gk \tanh(kh) \tag{6}$$

in which the angular wave frequency σ is related to the wave period, in this case T_m , by $\sigma = 2\pi/T_m$ (Hz); the angular wave number k is related to λ by $k = 2\pi/L$ (1/m); and g is the gravitational acceleration (m/s^2).

Thus, the characteristics of the regular waves representative of the sea state, which were used for the spatial discretization of the computational domain, were as follows: significant height, $H_s = 0.90$ m; length, $\lambda = 45.9915$ m; mean period, $T_m = 5.70$ s; and depth, $h = 10.976$ m.

Bathymetry Influence Study and Numerical Model Verification

This study was subdivided into two moments. In the first, a bathymetry study was performed with the objective of evaluating the bathymetry influence on the generation and propagation of realistic irregular waves, and, in the second, the verification of the generation of waves by means of the WaveMIMO methodology was performed. For this purpose, two computational domains were considered for the two-dimensional numerical wave channel. The first one (Figure 5a) presented a horizontal bottom (i.e., without bathymetry) and the second one (Figure 5b) presented the bathymetry found in the studied place, which was obtained from the nautical charts of the Directorate of Hydrography and Navigation of the Brazilian Navy [36] and catalogued by Cardoso [37]. For both cases, the wave channel presented a length of $L_c = 229.56$ m, which corresponded to 5λ , following the recommendation of Gomes et al. [38], and a height of $H_c = 15$ m. In addition, a constant water depth of $h = 10.976$ m for the domain without bathymetry was adopted, and a variable depth was employed for the domain with bathymetry, where the left side of the wave channel measured $h = 10.976$ m and the right side measured $h_1 = 10.520$ m.

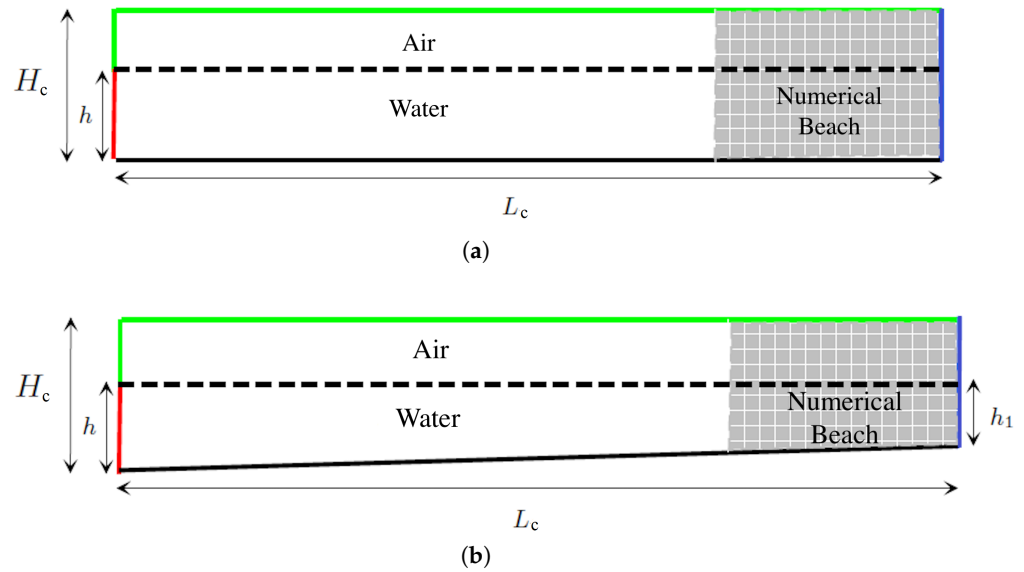


Figure 5. Schematic representations of computational domains for the bathymetry influence study. (a) Domain without bathymetry; (b) Domain with bathymetry.

As for the boundary conditions, in both cases, the following were used: atmospheric pressure (green line); wall (continuous black line), where the velocities were considered null; hydrostatic profile (blue line); and velocity inlet (red line), which was subdivided into 14 segments of size $h/14$, as recommended by Machado et al. [33]. It is important to mention that a numerical beach was used in the computational domain, in which a damping sink term was added to Equation (3), being defined as [28,39]

$$S = - \left[C_1 \rho V + \frac{1}{2} C_2 \rho |V| V \right] \left(1 - \frac{z - z_{fs}}{z_b - z_{fs}} \right) \left(\frac{x - x_s}{x_e - x_s} \right)^2 \quad (7)$$

in which C_1 is the linear damping coefficient (s^{-1}), C_2 is the quadratic damping coefficient (m^{-1}), V is the fluid velocity at a given point (m/s), and z_{fs} , z_b , x_e , and x_s are the free surface, bottom, starting, and ending points of the numerical beach domain (m), respectively.

The numerical beach tool can be used to absorb wave energy and reduce the effects of reflection, which is caused by the incidence of waves on the right wall of the channel. The damping coefficients, following recommendations from previous studies [39], were defined as $C_1 = 20 s^{-1}$ and $C_2 = 0 m^{-1}$, and the numerical beach length was defined as 2λ , i.e., $L_{nb} = 91.82 m$.

Regarding the spatial discretization, a stretched mesh was used [40]. For this, the computational domain was subdivided into 3 vertical regions with the following discretizations: 60 computational cells in the region that contained only water; 40 cells in the free surface region (air/water interface); and 20 cells in the region containing only air. Horizontally, the computational domain was subdivided into 250 computational cells, i.e., 50 cells per wavelength. Regarding temporal discretization, a time step of $\Delta t = 0.05 s$ was considered, as recommended by Machado et al. [33]. The total simulation time considered was 200 s of wave generation and propagation in the channel.

2.3. Geometric Optimization of OWC WEC

Following the bathymetry influence study, the OWC WEC device was inserted into the wave channel and its geometry was analyzed. To do so, the constructal design method was employed, which is based on the constructal theory. The constructal theory, developed by Adrian Bejan [22], explains how the generation of structures subjected to flow, such as those commonly found in nature, can be based on the principle of access to flow over time.

There are several studies that have used the constructal design in the geometric optimization of OWC devices under the incidence of regular waves (for instance, [41–43]), allowing the evaluation and improvement of the conversion of the energy contained in sea waves into electrical energy. In this study, the constructal design method, which was used to define the search space, was employed with an exhaustive search technique to obtain the optimized geometric shape of an OWC WEC device subjected to the sea state found in the city of Tramandaí, in the state of Rio Grande do Sul, Brazil.

For the constructal design application, it was necessary to define a performance indicator, the degrees of freedom, and restrictions. In this case, the performance indicator was the available hydropneumatic power, which must be maximized. The varied degree of freedom was the ratio H_1/L , being H_1 the height and L the length of the device's hydropneumatic chamber. Two degrees of freedom were kept constant, $H_2/l = 4.03$, which defines the ratio between the height and length of the turbine duct, and the submersion depth of the chamber $H_3 = 6.12$ m. These dimensions can be seen in Figure 6.

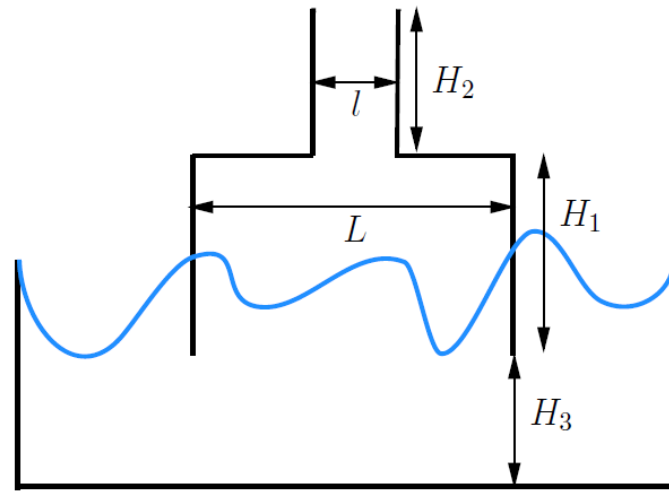


Figure 6. OWC device dimensions.

In this study, the geometric constraints were the volume of the hydropneumatic chamber, V_{ch} , and the total volume of the OWC, V_t , which were kept constant and are given by:

$$V_{ch} = H_1LL_1 \tag{8}$$

$$V_t = V_{ch} + H_2lL_1 \tag{9}$$

The third dimension L_1 had a unitary value, as the computational modeling adopted was two-dimensional. From Equation (8), it was possible to find formulations for the length, L , and height, H_1 , of the hydropneumatic chamber:

$$L = \sqrt{\frac{V_{ch}}{\left(\frac{H_1}{L}\right)L_1}} \tag{10}$$

$$H_1 = L\left(\frac{H_1}{L}\right) \tag{11}$$

The present study was based on Maciel [15], where the geometry of the OWC WEC was optimized considering the sea state found in the city of Rio Grande, in the state of Rio Grande do Sul, Brazil. Therefore, the same values of the degree of freedom H_1/L evaluated in that study were considered here. It is worth noting that the main difference between the studies was the location of the device and, consequently, the time series of irregular waves

to which the OWC WEC was subjected. Therefore, similar to Maciel [15], the device used was based on the dimensions of the OWC located in Pico Island, Azores, Portugal, with the following dimensions: $L = 12$ m; $H_1 = 13.4$ m; $l = 2.8$ m; $H = 11.3$ m; and $H_3 = 6.12$ m (see Figure 6).

Table 1 shows the cases defined by means of the constructal design application (variation of the ratio H_1/L) and its respective dimensions. As already stated, the value of H_3 remained constant, equal to 6.12 m. It is important to mention that ratio $H_1/L = 0.1985$ was the optimal case found in Maciel [15] and ratio $H_1/L = 1.1167$ was the reference case with the dimensions of the Pico OWC device.

Table 1. Configurations of the geometries used in the study.

H_1/L	H_1 (m)	L (m)
0.1985	5.65	28.46
0.4297	8.31	19.34
0.6608	10.31	15.16
0.8920	11.98	13.43
1.1167	13.40	12.00
1.3543	14.76	10.90
1.5854	15.97	10.07
1.8166	17.09	9.41
2.0478	18.15	8.86
2.2789	19.14	8.40

Regarding the computational domain, the OWC WEC was inserted in the wave channel in which the bottom of the channel presented bathymetry (see Figure 5b), according to the results from the bathymetry influence study. Furthermore, as recommended by De Lima [9], the OWC WEC was placed at 1.5λ from the beginning of the wave channel. Regarding the boundary conditions, they were the atmospheric pressure (green line), wall (continuous black line), hydrostatic profile (blue line), and velocity inlet (red line), which, as in the bathymetry influence study, it was subdivided into 14 segments of size $h/14$, as recommended by Machado et al. [33]. An illustration of the computational domain considering the OWC WEC is presented in Figure 7. Again, the numerical beach was used (Equation (7)).

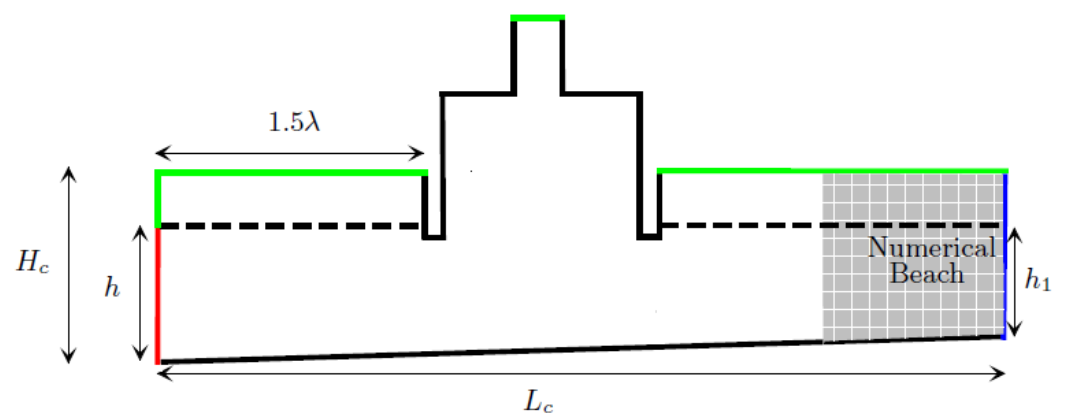


Figure 7. Computational domain used in the study cases.

Regarding the spatial discretization, a stretched mesh was used for the regions both before and after the device [40], as performed in the bathymetry influence study. For the discretization of the device, square-shaped cells with a size of 0.1 m were used and the thickness of its wall was 0.1 m, as recommended by De Lima [9]. As for temporal discretization, the time step $\Delta t = 0.05$ s was used [33]. In this study, the total simulation time was expanded to 900 s of wave generation in the channel in order to compare the results obtained with those of Maciel [15].

2.4. Error Metrics

To analyze the quality of the results, the mean absolute error, MAE, and root mean square error, RMSE, metrics were considered, respectively, given by [44]:

$$MAE = \frac{1}{n} \sum_{i=1}^n |O_i - R_i| \tag{12}$$

$$RMSE = \sqrt{\frac{1}{n} \sum_{i=1}^n |O_i - R_i|^2} \tag{13}$$

in which O_i represents the value found numerically, R_i represents the value used as a reference, and n represents the total number of data.

To monitor the free water surface elevation, vertical numerical probes were used, in which the integral was calculated by [28]:

$$\int \phi dA = \sum_{i=1}^n \phi_i |A_i| \tag{14}$$

in which ϕ_i is a variable field and A_i is the area of each computational cell volume (m^2). In the study of the influence of bathymetry, numerical probes were placed at $x = 0.000000, 10.455425, 20.910851, 31.366276, 41.821702, 50.186042, 60.641468, 71.096893, 81.552318, 92.007744, \text{ and } 102.463169$ m, and in the geometric optimization study of the OWC WEC, the numerical probe was positioned at the center of the device, i.e., $x = (1.5\lambda + L/2)$ m.

To monitor the static pressure and air mass flow rate, a horizontal numerical probe was used at the center of the OWC turbine duct, i.e., $x \in [1.5\lambda + L/2 - 1.4, 1.5\lambda + L/2 + 1.4]$, in which the integrals were calculated, respectively, by [28]:

$$\frac{1}{A} \int \phi dA = \frac{1}{A} \sum_{i=1}^n \phi_i |A_i| \tag{15}$$

$$\int \rho_{air} \vec{v} \cdot d\vec{A} = \sum_{i=1}^n \rho_{air} \vec{v}_i \cdot \vec{A}_i \tag{16}$$

in which \vec{v} represents the velocity vector on the face (m/s) and ρ_{air} the air density (kg/m^3).

It is important to mention that the position of the numerical probes inside the device changed according to the geometric configurations. With this, it was possible to calculate the available hydropneumatic power, which is given by [45]:

$$P_H = \left(p + \frac{1}{2} \rho_{air} v_{air}^2 \right) \frac{\dot{m}}{\rho_{air}} \tag{17}$$

in which p is the static pressure in the duct (Pa), v_{air} is the air velocity in the duct (m/s), and \dot{m} is air mass flow rate inside the turbine duct (kg/s).

Finally, to quantitatively evaluate the available power of the geometries studied and determine the ratio H_1/L that maximized its value, the root mean square, RMS, was used [46]:

$$P_{RMS} = \sqrt{\frac{1}{n} \sum_{k=1}^n P_k^2} \tag{18}$$

in which P_k indicates the instantaneous available power (W) calculated in each time step.

3. Results and Discussion

3.1. Study of Bathymetry Influence in the Generation and Propagation of Realistic Irregular Waves and Numerical Model Verification

As earlier mentioned, the study of bathymetry considering realistic irregular waves was divided into two cases. In the first case, the channel presented a horizontal bottom, i.e., without bathymetry, and the second case presented a sloped bottom, reproducing the bathymetry found in the study area (see Figure 5). Aiming to evaluate the difference in wave propagation in channels with and without bathymetry, Table 2 presents the metrics MAE and RMSE monitored at 11 points of the bathymetry. The results obtained in the numerical simulation that considered the wave channel bathymetry were taken as a reference, as it represented the computational domain that most closely resembled the simulation performed in TOMAWAC, which originated the boundary conditions imposed in Fluent, being more similar to the reality of the study area.

Table 2. MAE and RMSE results considering the bathymetry cases subjected to realistic irregular waves.

Probe Position (m)	MAE (m)	RMSE (m)
0.000000	0.004264	0.006133
10.455425	0.019815	0.020653
20.910851	0.019803	0.020501
31.366276	0.019803	0.020468
41.821702	0.019835	0.020556
50.186042	0.019836	0.020555
60.641468	0.019802	0.020494
71.096893	0.019757	0.020514
81.552318	0.019746	0.020618
92.007744	0.019743	0.020814
102.463169	0.019682	0.021028

As expected, the smallest differences were found in the wave generation zone ($x = 0$ m), as it was the location in the wave channel that was least influenced by the bathymetry. Next, it was observed that the largest differences in MAE and RMSE, respectively, occurred at positions $x = 50.186042$ m and 102.463169 m. When comparing them with the significant wave height of the regular waves representative of this sea state, differences of approximately 2.2% were found in both metrics, which confirmed that, in the analyzed situation, the use of bathymetry did not have a significant influence on the generation and propagation of realistic irregular waves.

Figures 8a and 8b present, respectively, the comparison between the free surface elevation of realistic irregular waves at positions $x = 0$ m and 71.096893 m. It is worth noting that these positions were chosen for evaluation due to the fact that the generation of realistic irregular waves occurred at $x = 0$ m, whereas, at $x = 71.096893$ m, the OWC WEC was inserted into the wave channel, as recommended by De Lima [9].

Figure 8a shows the waves numerically generated (using Fluent) in the wave channels with and without bathymetry, along with the free surface elevation from TOMAWAC, allowing the verification of the wave generation. As can be observed, the waves generated in the wave channels with and without bathymetry adequately represented the sea state from TOMAWAC. To confirm the observed qualitative results, the free surface elevations obtained with Fluent were compared with those from TOMAWAC using the MAE and RMSE metrics. For the case of the wave channel with bathymetry, the differences were found to be 0.0999 m and 0.1285 m, respectively, while, for the wave channel without bathymetry, the differences were 0.1003 m and 0.1288 m, respectively. These results are in agreement with those found by Machado et al. [33] and confirm the appropriate generation of realistic irregular waves in both wave channels, with and without bathymetry. Furthermore, as observed in Figure 8a, the free surface elevations monitored in the generation zone

for the channels with and without bathymetry were similar. When comparing the MAE and RMSE metrics presented in Table 2 (for $x = 0$ m) with the significant wave height of the regular waves representative of this sea state, differences of 0.47% and 0.68%, respectively, were found.

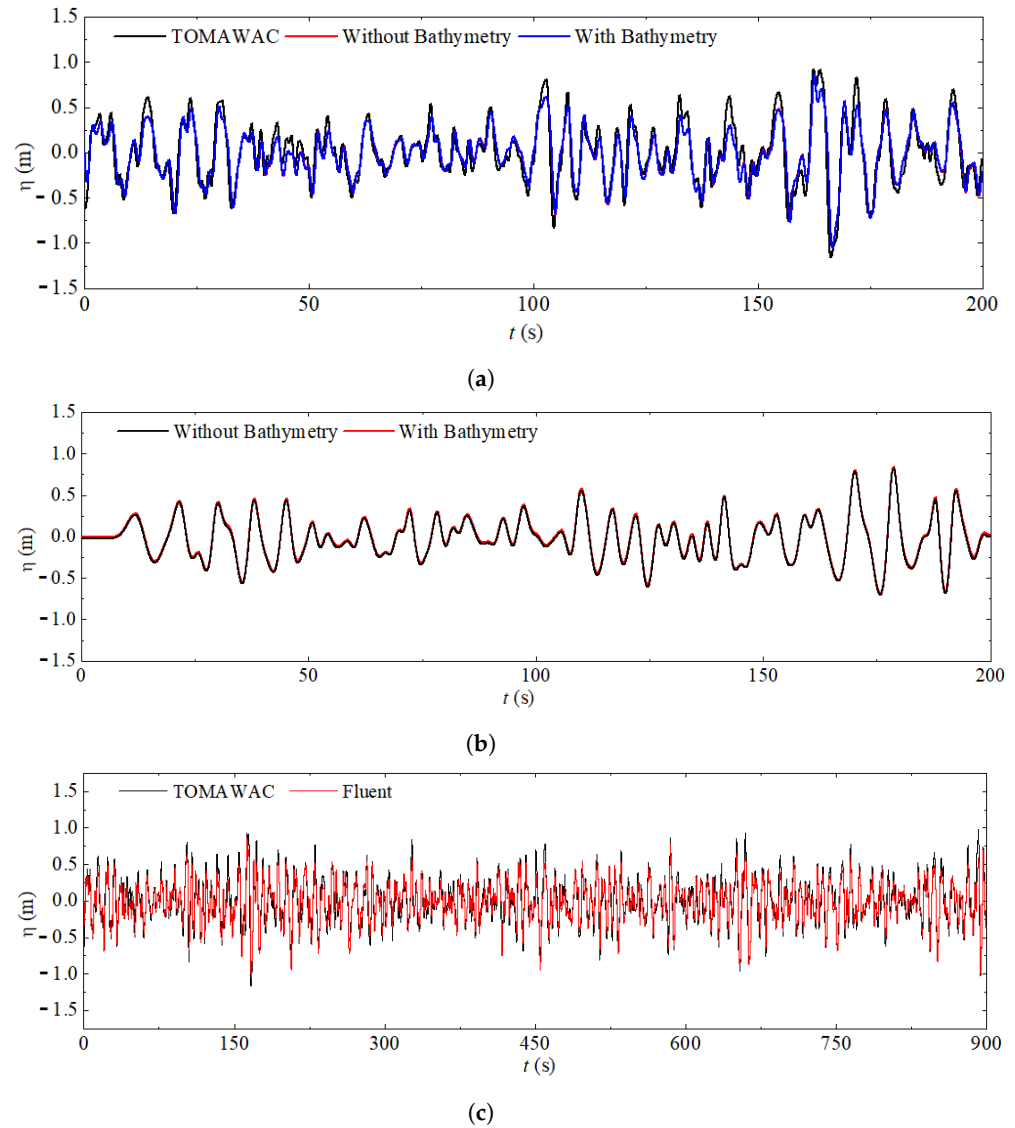


Figure 8. Free surface elevation considering (a) 200 s of wave generation monitored in probe localized at $x = 0$ m; (b) 200 s of wave propagation monitored in probe localized at $x = 71.096893$ m; (c) 900 s of wave generation monitored in probe localized at $x = 0$ m.

Figure 8b, on the other hand, shows the monitored free surface elevation at the probe located at $x = 71.096893$ m in both wave channels, with and without bathymetry. Qualitatively, it is evident that the propagation of realistic irregular waves was not significantly influenced by the wave channel bathymetry. Quantitatively, when comparing the MAE and RMSE metrics with the significant wave height of the regular waves representative of this sea state, differences of approximately 2.2% were found again. Based on the results obtained, the bathymetry was taken into consideration for the simulations of the OWC WEC device.

Lastly, aiming to compare the results obtained for the OWC WEC in the present study with those found in Maciel [15], Figure 8c presents the verification of 900 s of wave generation in the channel with bathymetry. For this purpose, the monitored free surface elevation in the wave generation zone ($x = 0$ m) was compared to the elevation from

TOMAWAC at the same position. Here, MAE and RMSE values of 0.0814 m and 0.1044 m, respectively, were found. It should be noted that realistic irregular waves were properly generated using the WaveMIMO methodology [33], as evidenced by the low error metric values obtained.

3.2. Study of Geometric Optimization of OWC WEC Subjected to Realistic Irregular Waves

The OWC WEC device was introduced in the wave channel with bathymetry (see Figure 7), in which it was possible to carry out the geometric optimization of the device and to maximize the available hydropneumatic power, considering the 10 configurations listed in Table 1, under the influence of realistic irregular waves, as can be seen in Figures 9 and 10.

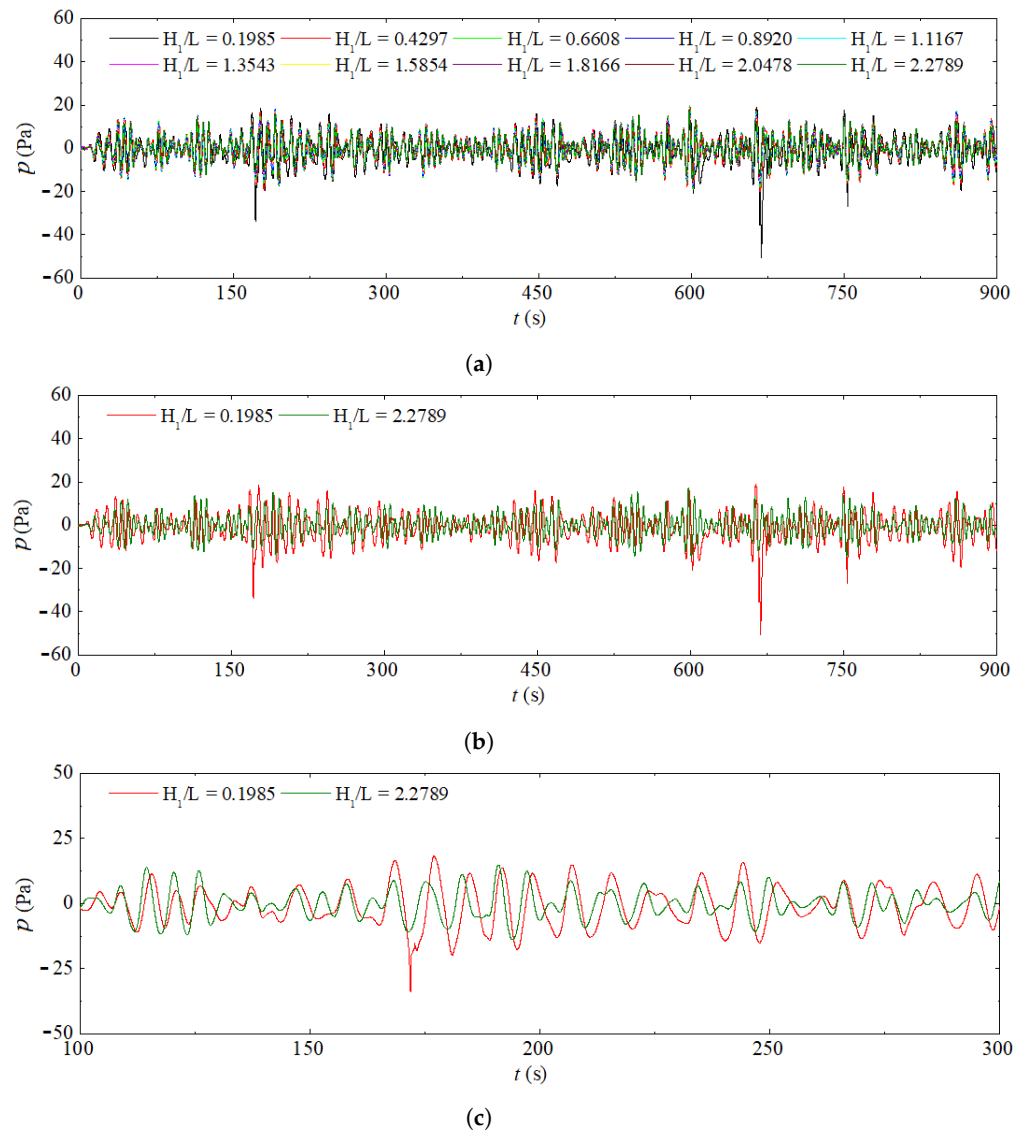


Figure 9. Static pressure for (a) all the evaluated geometric configurations while $t \leq 900$ s; (b) $H_1/L = 0.1985$ and 2.2789 while $t \leq 900$ s; (c) $H_1/L = 0.1985$ and 2.2789 while $100 \text{ s} \leq t \leq 300$ s.

Figure 9a shows the variation in static pressure that occurred during the 900 s of simulation for all H_1/L ratios. Meanwhile, in Figure 9a, it is possible to observe the variation in static pressure that occurred at $t \leq 900$ s for the ratio that qualitatively presented the best result, $H_1/L = 0.1985$, and for the ratio that qualitatively presented the worst result, $H_1/L = 2.2789$. Next, Figure 9c presents the same cases as Figure 9b, in a specific time interval of $100 \text{ s} \leq t \leq 300$ s, which was when the second highest pressure peak occurred, among the 900 s of simulation. As can be observed in Figure 9a, the results for

all H_1/L ratios analyzed exhibited similar behavior, except for the case $H_1/L = 0.1985$, which presented higher static pressure peaks compared to the others. This can be justified by the fact that, for this ratio, L is larger (see Table 1), causing the greater compression and decompression of the air inside the hydropneumatic chamber. It is important to highlight that this fluid dynamic behavior was also observed in previous works, such as De Lima et al. [12] and Gomes et al. [41]. As seen in Figure 9b, for $H_1/L = 0.1985$, the highest static pressure peak occurred during the decompression of the hydropneumatic chamber, at $t = 668.55$ s, and corresponded to -50.481 Pa. Meanwhile, for $H_1/L = 2.2789$, the highest static pressure peak was 17.2 Pa and occurred during the compression, at $t = 597.85$ s. In Figure 9c, the second highest static pressure peak can be observed at $t = 171.85$ s and 191 s for $H_1/L = 0.1985$ and 2.2789 , respectively. There is a difference of 61% between these static pressure peaks. Additionally, it can be observed that the smallest H_1/L ratios resulted in the highest static pressure peaks, either during compression or decompression of the hydropneumatic chamber of the OWC WEC, and these peaks stabilized as the H_1/L values increased.

Figure 10a shows the variation in the available hydropneumatic power for all H_1/L ratios during the 900 s of simulation. Meanwhile, in Figure 10b, it is possible to observe the variation in hydropneumatic power that occurred at $t \leq 900$ s for the ratio that presented the best qualitative results, $H_1/L = 0.1985$, and for $H_1/L = 2.2789$, which presented the worst qualitative results. Next, Figure 10c shows the ratios $H_1/L = 0.1985$ and 2.2789 for $100 \text{ s} \leq t \leq 300 \text{ s}$, the interval during which one of the highest peaks in hydropneumatic power occurred among the 900 s of simulation.

As can be observed in Figure 10a,b, the highest peak in hydropneumatic power found, $P_H = 279.98$ W, occurred during the compression of the hydropneumatic chamber, for the ratio $H_1/L = 0.1985$, at $t = 668.95$ s. Additionally, the second highest peak in hydropneumatic power was also found for $H_1/L = 0.1985$, which occurred during the decompression of the hydropneumatic chamber ($t = 667$ s) and was equal to -236.61 W. On the other hand, the highest peak in hydropneumatic power for $H_1/L = 2.2789$ occurred at $t = 598.6$ s and was 75.5% and 71.1% lower than the highest and second highest peaks in hydropneumatic power found for $H_1/L = 0.1985$, respectively. In Figure 10c, it is confirmed that the peaks in hydropneumatic power for $H_1/L = 0.1985$ were prominent compared to those found for $H_1/L = 2.2789$, confirming that this case presented the best results.

Figure 11 relates the values of P_{RMS} obtained in the present study with those found in Maciel [15]. In both studies, the case that optimized the available hydropneumatic power was $(H_1/L)_o = 0.1985$. It is noteworthy that the RMS hydropneumatic power found in this study was 25.44 W, representing a 14.14% loss in device efficiency compared to the power found by Maciel [15].

It is worth noting that the case with H_1/L ratio = 1.1167 represented the dimensions of the OWC WEC installed at Pico Island. For this case, a hydropneumatic RMS power of 14.88 W was obtained, a value 20.09% larger than that found by Maciel [15], which was 11.89 W. As for the worst efficiency, it was found for $H_1/L = 2.2789$ in both studies. However, in this study, the minimum RMS hydropneumatic power was found to be 38.74% higher than the value found in Maciel [15], which was 6.83 W.

Finally, the optimal case found in this study, $(H_1/L)_o = 0.1985$, was 2.28 times more efficient than the worst case, $H_1/L = 2.2789$. Furthermore, as H_1/L increased, the RMS hydropneumatic power decreased, which was also observed in Maciel [15]. Additionally, it could be concluded that even with the OWC WEC subjected to different wave elevation series, the geometric evaluations showed similar curves, which can be justified by the significant similarity between the wave climate behavior in Rio Grande and Tramandaí [47].

Figure 12 depicts the phase topology, in which water and air are represented in red and blue colors, respectively. In Figure 12a–d, the case of optimal geometric configuration $(H_1/L)_o = 0.1985$ is shown, while, in Figure 12e–h, the worst case, $H_1/L = 2.2789$, is presented. In Figure 12a,e, the initial instant ($t = 0$ s) of the simulation is shown, where the flow was at rest and, therefore, there was no incidence of irregular waves into the

hydropneumatic chamber of the OWC WEC. Next, Figure 12b,f shows the flow behavior at $t = 300$ s, a moment where a larger volume of water could be observed inside the device chamber for the optimal case, in contrast to the worst case (Figure 12f), in which there was less oscillatory movement. Figure 12c,g depicts $t = 600$ s, a moment that, similar to the previous $t = 300$ s, shows a higher volume of water in the hydropneumatic chamber for the case $(H_1/L)_o = 0.1985$ compared to $H_1/L = 2.2789$, confirming the results presented in Figure 11. Finally, Figure 12d,h shows the final instant of the simulation, $t = 900$ s, where once again it can be observed that the optimal case presented a larger volume of water in the hydropneumatic chamber compared to the case with $H_1/L = 2.2789$. It is important to highlight that, during compression, wave crests could be observed inside the device, while, during decompression, wave troughs were visible. The alternating motion of the waves inside the hydropneumatic chamber of the device led to alternating air flow in the turbine duct, where the turbine was installed, converting kinetic energy into electrical energy.

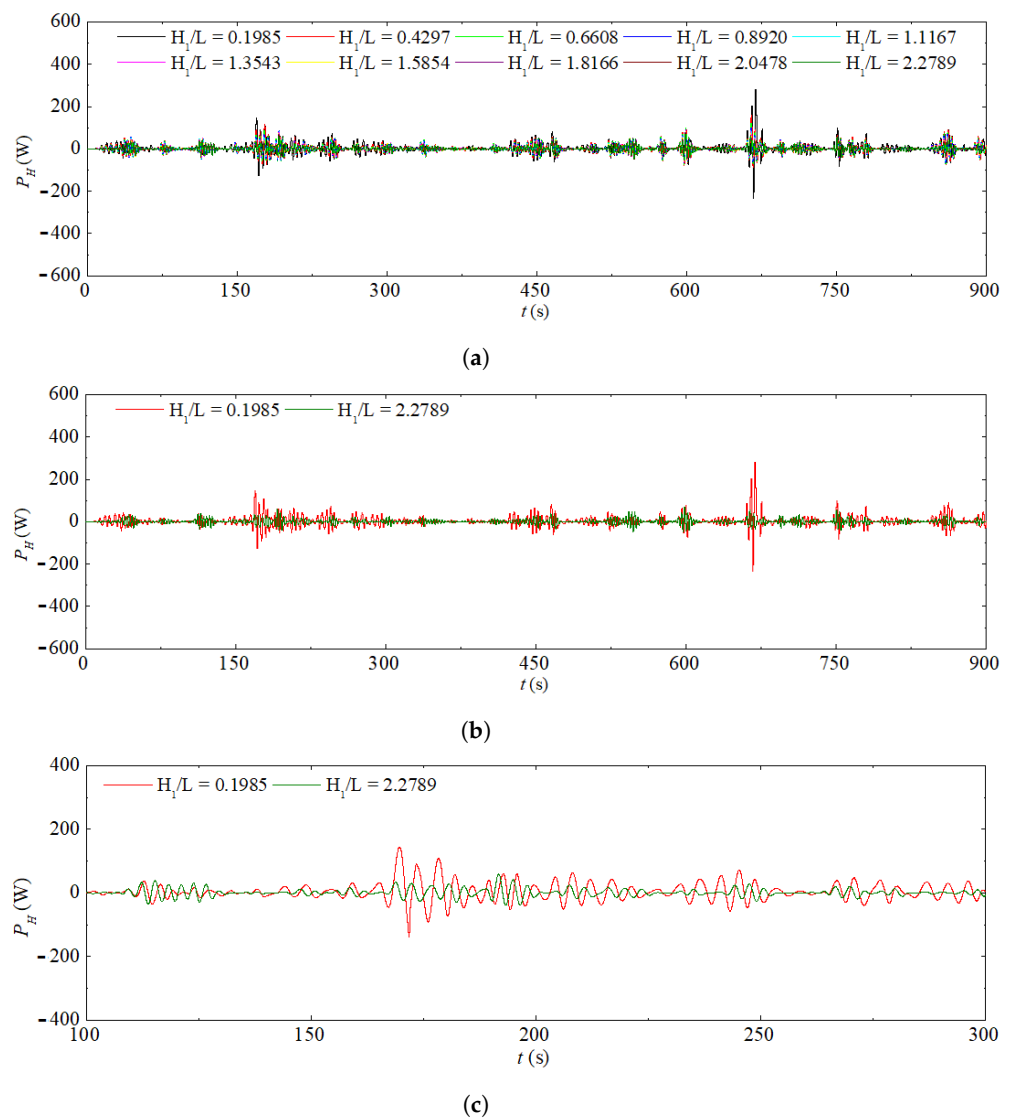


Figure 10. Available hydropneumatic power of (a) all the evaluated geometric configurations while $t \leq 900$ s; (b) $H_1/L = 0.1985$ and 2.2789 while $t \leq 900$ s; (c) $H_1/L = 0.1985$ and 2.2789 while $100 \text{ s} \leq t \leq 300$ s.

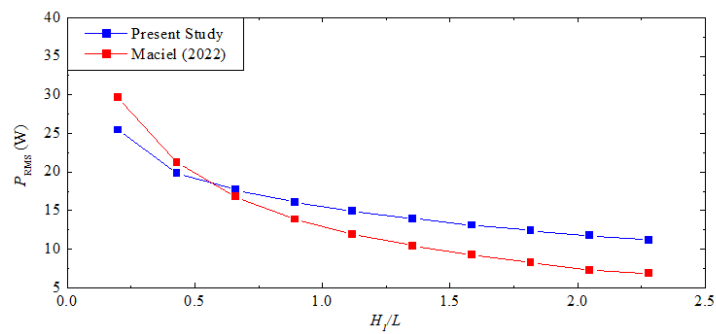


Figure 11. Comparison of P_{RMS} values between this study and Maciel [15].

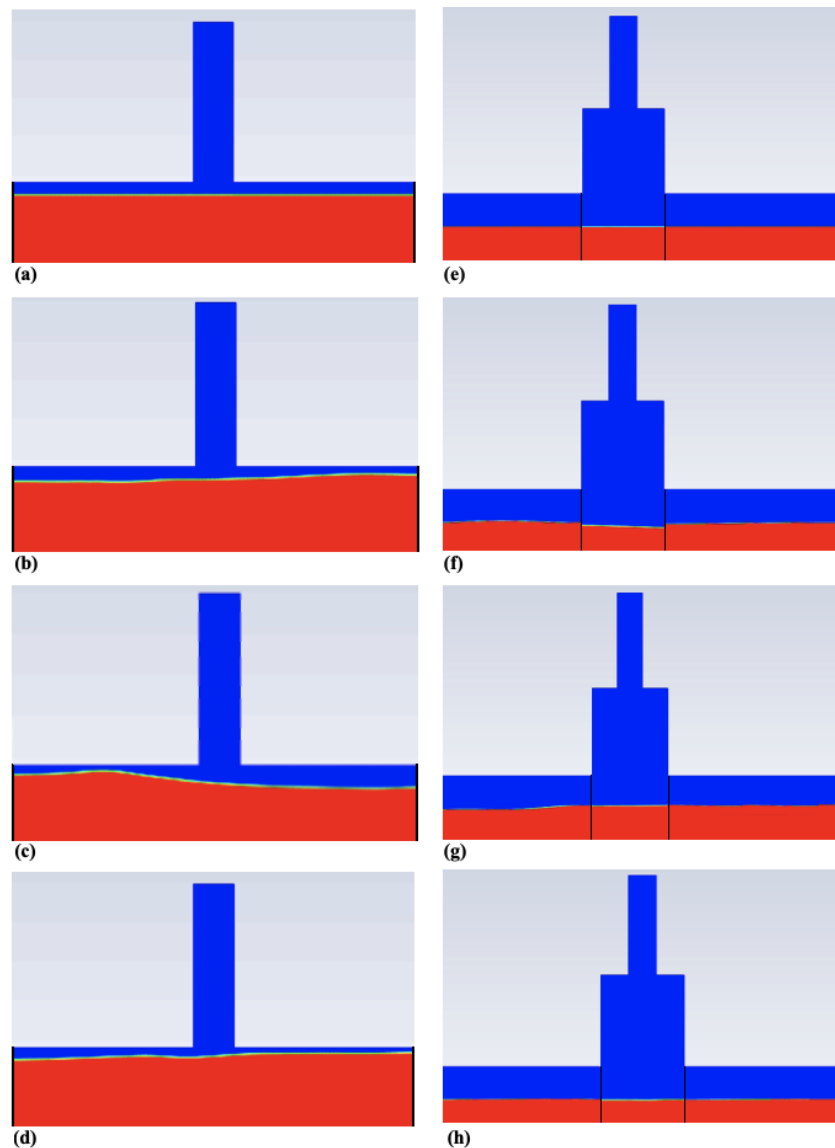


Figure 12. Flow behavior in the device for the optimal case $(H_1/L)_o = 0.1985$ at (a) $t = 0$ s, (b) $t = 300$ s, (c) $t = 600$ s, and (d) $t = 900$ s, and for the worst case $H_1/L = 2.2789$ at (e) $t = 0$ s, (f) $t = 300$ s, (g) $t = 600$ s, and (h) $t = 900$ s.

4. Conclusions

Regarding the study of bathymetry influence, concerning the generation of realistic irregular waves, the best results were achieved with the bathymetric channel. However, in the propagation of realistic irregular waves, there was no significant difference in the free

water surface elevation whether the bathymetry was considered or not. Therefore, the local bathymetry was used to verify the generation of a realistic sea state found in Tramandaí.

Next, a geometric optimization study of an OWC WEC device was carried out, taking into account the wave climate and local bathymetry. The optimal geometry that maximized the available hydropneumatic power in the converter presented a ratio of $(H_1/L)_o = 0.1985$, in which case $H_1 = 5.65$ m and $L = 28.46$ m. The RMS hydropneumatic power found when considering this geometric configuration was 25.44 W, which was 2.28 times more efficient than the worst-case scenario, $H_1/L = 2.2789$. Furthermore, by analyzing the 10 investigated geometries, it was observed that the degree of freedom H_1/L and the RMS hydropneumatic powers found were inversely proportional. In other words, as the H_1/L ratio increased, the P_{RMS} decreased, which was a behavior trend analogous to those observed in previous works, as in Maciel [15].

For future studies, an investigation regarding the influence of bathymetry on the representative regular waves generated through the WaveMIMO methodology can be suggested. Additionally, one could reproduce the geometric optimization carried out in this study considering representative regular waves of this sea state, as a means to investigate whether the optimal geometry would be influenced by the wave climate.

Author Contributions: Conceptualization, A.P.G.M., J.S.Z., L.A.I. and B.N.M.; methodology, A.P.G.M., J.S.Z., L.A.I. and B.N.M.; software, A.P.G.M. and B.N.M.; validation, A.P.G.M., B.N.M. and L.A.I.; formal analysis, B.N.M. and L.A.I.; investigation, A.P.G.M., B.N.M. and L.A.I.; resources, L.A.O.R., E.D.d.S., J.S.Z., B.N.M. and L.A.I.; data curation, A.P.G.M. and B.N.M.; writing—original draft preparation, A.P.G.M., R.P.M., B.N.M. and L.A.I.; writing—review and editing, R.P.M., P.H.O., B.N.M., L.A.I., L.A.O.R., E.D.d.S. and J.S.Z.; visualization, B.N.M. and L.A.I.; supervision, B.N.M., L.A.I. and J.S.Z.; project administration, B.N.M. and L.A.I.; funding acquisition, B.N.M., L.A.I., L.A.O.R. and E.D.d.S. All authors have read and agreed to the published version of the manuscript.

Funding: This research was funded by the Brazilian Coordination for the Improvement of Higher Education Personnel—CAPES (Finance Code 001), the Research Support Foundation of the State of Rio Grande do Sul—FAPERGS (Public Call FAPERGS 07/2021—Programa Pesquisador Gaúcho—PqG— 21/2551-0002231-0), and the Brazilian National Council for Scientific and Technological Development—CNPq (Processes: 309648/2021-1, 307791/2019-0, 308396/2021-9, 440010/2019-5, and 440020/2019-0), and we also thank UFRGS for the financial support (Edital PROPESQ/UFRGS 2019—Programa Institucional de Auxílio à Pesquisa de Docentes Recém—Contratados pela UFRGS).

Institutional Review Board Statement: Not applicable.

Informed Consent Statement: Not applicable.

Data Availability Statement: The data presented in this study are available on request from the corresponding author. The data are not publicly available due to privacy reasons.

Acknowledgments: Mocellin, A.P., thanks CAPES for the Master's Dissertation Scholarship; Maciel, R., thanks CNPq for the Master's Dissertation Scholarship (Chamada CNPq/EQUINOR Energia Ltda. 2018, process 440020/2019-0).

Conflicts of Interest: The authors declare no conflicts of interest. The funders had no role in the design of the study; in the collection, analyses, or interpretation of data; in the writing of the manuscript; or in the decision to publish the results.

Abbreviations

The following abbreviations are used in this manuscript:

CFD	Computational fluid dynamics
FVM	Finite volume method
MAE	Mean absolute error
MWL	Mean water level
OWC	Oscillating water column
PISO	Pressure-implicit splitting of operators

PRESTO	Pressure staggering option
RMSE	Root mean square error
TOMAWAC	Telemac-based operational model addressing wave action computation
VOF	Volume of fluid
WEC	Wave energy converter
Nomenclature	
A	Amplitude of the wave [m]
A_i	Area of each computational cell volume [m ²]
α	Volumetric fraction [-]
α_{air}	Volumetric fraction of air [-]
α_{water}	Volumetric fraction of water [-]
C_1	Linear damping coefficient [s ⁻¹]
C_2	Quadratic damping coefficient [m ⁻¹]
Δt	Time step [s]
η	Free surface elevation [m]
\vec{g}	Gravity acceleration [m/s ²]
h	Water depth [m]
H	Wave height [m]
H_c	Height of wave channel [m]
H_s	Significant height [m]
H_1	Height of the hydropneumatic chamber [m]
H_2	Height of the turbine duct [m]
H_3	Submersion depth of OWC [m]
k	Angular wave number [1/m]
L	Length of the hydropneumatic chamber [m]
l	Length of the turbine duct [m]
L_c	Length of the wave channel [m]
L_{nb}	Length of the numerical beach [m]
λ	Wavelength [m]
\dot{m}	Air mass flow rate [kg/s]
μ	Viscosity [kg/m.s]
n	Number of data [-]
O_i	Numerical value [-]
p	Static pressure [Pa]
P_k	Instantaneous available power [W]
ϕ_i	Variable field [-]
ρ_{air}	Air density [kg/m ²]
ρ	Density [kg/m ³]
R_i	Reference value [-]
S	Source term [N/m ²]
σ	Angular wave frequency [Hz]
T	Period [s]
T_m	Mean period [s]
t	Time [s]
$\bar{\tau}$	Strain rate tensor [N/m ²]
u	Horizontal velocity [m/s]
V	Fluid velocity [m/s]
\vec{v}	Velocity vector [m/s]
v_{air}	Air velocity in the duct [m/s]
V_{ch}	Volume of the hydropneumatic chamber [m ³]
V_t	Total volume of the OWC [m ³]
w	Vertical velocity [m/s]
x	Numerical probe position [m]
x_e	Starting point [m]
x_s	Ending point [m]
z_{fs}	Free surface point [m]
z_b	Bottom point [m]

References

1. Oliveira, J.F.G.D.; Trindade, T.C.G. Sustainability Performance Evaluation of Renewable Energy Technologies. In *Sustainability Performance Evaluation of Renewable Energy Sources: The Case of Brazil*; Springer: Berlin/Heidelberg, Germany, 2018.
2. IPCC. *Renewable Energy Sources and Climate Change Mitigation: Special Report of the Intergovernmental Panel on Climate Change*; Cambridge University Press: Cambridge, UK, 2012.
3. WEC. *World Energy Resources*; WEC: London, UK, 2016.
4. Tolmasquim, M.T. *Energia Renovável: Hidráulica, Biomassa, Eólica, Solar, Oceânica*; Empresa de Pesquisa Energética (EPE): Rio de Janeiro, Brazil, 2006. (In Portuguese)
5. Khan, N.; Kalair, A.; Abas, N.; Haider, A. Review of ocean tidal, wave and thermal energy technologies. *Renew. Sustain. Energy Rev.* **2017**, *72*, 590–604. [[CrossRef](#)]
6. Cruz, J. *Ocean Wave Energy: Current Status and Future Perspectives*, 1st ed.; Springer: Berlin/Heidelberg, Germany, 2008.
7. Falcão, A.F.; Henriques, J.C. Oscillating-water-column wave energy converters and air turbines: A review. *Renew. Energy* **2016**, *85*, 1391–1424. [[CrossRef](#)]
8. Gomes, M.N. Constructal Design de Dispositivos Conversores de Energia das Ondas do mar em Energia elétrica do Tipo Coluna de Água Oscilante. Ph.D. Thesis, Universidade Federal do Rio Grande do Sul, Porto Alegre, Brazil, 2014. (In Portuguese)
9. De Lima, Y.T.B. Análise Geométrica Através do Design Construtal de Conversores de Energia das Ondas do mar do Tipo Coluna de água Oscilante com Câmaras Hidropneumáticas Acopladas. Ph.D. Thesis, Universidade Federal do Rio Grande do Sul, Porto Alegre, Brazil, 2021. (In Portuguese)
10. Lorenzini, G.; Lara, M.F.E.; Rocha, L.A.O.; Gomes, M.N.; dos Santos, E.D.; Isoldi, L.A. Constructal design applied to the study of the geometry and submergence of an oscillating water column. *Int. J. Heat Technol.* **2015**, *33*, 31–38. [[CrossRef](#)]
11. De Lima, Y.T.B.; Rocha, L.A.O.; Gomes, M.N.; dos Santos, E.D. Aplicação Do Método Design Construtal Na Avaliação Numérica Da Potência Hidropneumática De Um Dispositivo Conversor De Energia Das Ondas Do Mar Do Tipo Coluna De Água Oscilante Com Região De Transição Trapezoidal. *Rev. Bras. Energias Renov.* **2017**, *6*, 376–396. (In Portuguese) [[CrossRef](#)]
12. De Lima, Y.T.B.; Gomes, M.N.; Cardozo, C.F.; Isoldi, L.A.; dos Santos, E.D.; Rocha, L.A.O. Analysis of geometric variation of three degrees of freedom through the constructal design method for a oscillating water column device with double hidropneumatic chamber. *Defect Diffus. Forum* **2019**, *396*, 22–31. [[CrossRef](#)]
13. De Deus, M.J.; Souza, L.C.; Da Silva, M.O.A.; Do Amaral, C.H.A.P.; Dos Santos, E.D.; Isoldi, L.A.; Gomes, M.N. Aplicação de Design Construtal para a Análise Geométrica de um Dispositivo CAO com Formato de Duplo Trapézio Submetido a um Espectro do Tipo Pierson-Moskowitz. *Retec-Rev. Tecnol.* **2019**, *12*, 55–67. (In Portuguese)
14. Teixeira, P.R.F.; Didier, E. Numerical analysis of the response of an onshore oscillating water column wave energy converter to random waves. *Energy* **2021**, *1*, 11919. [[CrossRef](#)]
15. Maciel, R.P. Constructal Design Applied to an Oscillating Water Column Wave Energy Converter Device Subjected to a Realistic Sea State. Master's Thesis, Universidade Federal do Rio Grande, Porto Alegre, Brazil, 2022.
16. Mavrakos, A.S.; Konispoliatis, D.N.; Ntouras, D.G.; Papadakis, G.P.; Mavrakos, S.A. Hydrodynamics of Moonpool-Type Floaters: A Theoretical and a CFD Formulation. *Energies* **2022**, *15*, 570. [[CrossRef](#)]
17. Zabala, I.; Henriques, J.; Blanco, J.; Gomez, A.; Gato, L.; Bidaguren, I.; Falcão, A.; Amezaga, A.; Gomes, R. Wave-induced real-fluid effects in marine energy converters: Review and application to OWC devices. *Energy Rev.* **2019**, *11*, 535–549. [[CrossRef](#)]
18. Gomes, M.N.; dos Santos, E.D.; Isoldi, L.A.; Rocha, L.A.O. Two-Dimensional Geometric Optimization of an Oscillating Water Column Converter of Real Scale. In Proceedings of the 22nd International Congress of Mechanical Engineering, Ribeirão Preto, Brazil, 3–7 November 2013; pp. 3468–3479.
19. Gomes, M.N.; Rocha, L.A.O.; Waess, K.R.; Isoldi, L.A.; dos Santos, E.D. Modelagem Computacional e Otimização Geométrica 2D com Constructal Design de um Dispositivo do Tipo Coluna de Água Oscilante em Escala Real—Comparação Onshore E Offshore. In Proceedings of the XXXIV Iberian Latin-American Congress on Computational Methods in Engineering, Pirenópolis, Brazil, 10–13 November 2013; pp. 1–20. (In Portuguese)
20. Martins, J.C.; Fragassa, C.; Goulart, M.M.; dos Santos, E.D.; Isoldi, L.A.; Gomes, M.N.; Rocha, L.A.O. Constructal Design of an Overtopping Wave Energy Converter Incorporated in a Breakwater. *J. Mar. Sci. Eng.* **2022**, *10*, 471. [[CrossRef](#)]
21. Seibt, F.M.; Isoldi, L.A.; dos Santos, E.D.; Rocha, L.A.O. Study of the Effect of the Relative Height on the Efficiency of a Submerged Horizontal Plate Type Wave Energy Converter Applying Constructal Design. In Proceedings of the XXXVIII Iberian Latin American Congress on Computational Methods in Engineering, Florianópolis, Brazil, 5–8 November 2017.
22. Bejan, A. *Shape and Structure, from Engineering to Nature*; Cambridge University Press: Cambridge, UK, 2000.
23. Pecher, A.; Kofoed, J.P. *Handbook of Ocean Wave Energy*; Springer: Berlin/Heidelberg, Germany, 2017.
24. Mahnamfar, F.; Altunkaynak, A. Comparison of numerical and experimental analyses for optimizing the geometry of OWC systems. *Ocean. Eng.* **2017**, *130*, 10–24. [[CrossRef](#)]
25. Liu, Z.; Cui, Y.; Xu, C.; Sun, L.; Li, M.; Jin, J. Experimental and numerical studies on an OWC axial-flow impulse turbine in reciprocating air flows. *Renew. Sustain. Energy Rev.* **2019**, *113*, 109272. [[CrossRef](#)]
26. Gomes, M.N.; de Deus, M.J.; dos Santos, E.D.; Isoldi, L.A.; Rocha, L.A.O. Analysis of the Geometric Constraints Employed in Constructal Design for Oscillating Water Column Devices Submitted to the Wave Spectrum Through a Numerical Approach. *Defect Diffus. Forum* **2019**, *390*, 193–210. [[CrossRef](#)]

27. Dean, R.G.; Dalrymple, R.A. *Water Wave Mechanics for Engineers and Scientists*; World Scientific: Singapore, 1991.
28. ANSYS Inc. *Ansys Fluent Theory Guide*; ANSYS, Inc.: Cannonsburg, PA, USA, 2013.
29. Hirt, C.W.; Nichols, B.D. Volume of Fluid (VOF) Method for the Dynamics of Free Boundaries. *J. Comput. Phys.* **1981**, *39*, 201–225. [[CrossRef](#)]
30. Versteeg, H.K.; Malalasekera, W. *An Introduction to Computational Fluid Dynamics—The Finite Volume Method*; Pearson Education Limited: London, UK, 2007.
31. Srinivasan, V.; Salazar, A.J.; Saito, K. Modeling the disintegration of modulated liquid jets using volume-of-fluid (VOF) methodology. *Appl. Math. Model.* **2011**, *35*, 3710–3730. [[CrossRef](#)]
32. Cisco, L.A.; Maciel, R.P.; Oleinik, P.H.; dos Santos, E.D.; Gomes, M.N.; Rocha, L.A.O.; Isoldi, L.A.; Machado, B.N. Numerical Analysis of the Available Power in an Overtopping Wave Energy Converter Subjected to a Sea State of the Coastal Region of Tramandaí, Brazil. *Fluids* **2022**, *7*, 359. [[CrossRef](#)]
33. Machado, B.N.; Oleinik, P.H.; Kirinus, E.P.; dos Santos, E.D.; Rocha, L.A.O.; Gomes, M.N.; Conde, J.M.P.; Isoldi, L.A. WaveMIMO Methodology: Numerical Wave Generation of a Realistic Sea State. *J. Appl. Comput. Mech.* **2021**, *7*, 2129–2148. [[CrossRef](#)]
34. Maciel, R.P.; Fragassa, C.; Machado, B.N.; Rocha, L.A.O.; dos Santos, E.D.; Gomes, M.N.; Isoldi, L.A. Verification and Validation of a Methodology to Numerically Generate Waves Using Transient Discrete Data as Prescribed Velocity Boundary Condition. *J. Mar. Sci. Eng.* **2021**, *9*, 896. [[CrossRef](#)]
35. Oleinik, P.H.; Tavares, G.P.; Machado, B.N.; Isoldi, L.A. Transformation of Water Wave Spectra into Time Series of Surface Elevation. *Earth* **2021**, *2*, 997–1005. [[CrossRef](#)]
36. Directorate of Hydrography and Navigation of the Brazilian Navy. Nautical Charts | Navy Hydrography Center. Available online: <https://www.marinha.mil.br/chm/dados-do-segnav-cartas-nauticas> (accessed on 1 December 2022).
37. Cardoso, S.D.; Marques, W.C.; Kirinus, E.d.P.; Stringari, C.E. Levantamento batimétrico usando cartas náuticas. In Proceedings of the 13^a Mostra da Produção Universitária, Rio Grande: Universidade Federal do Rio Grande, Rio Grande, Brazil, 14 October 2014; p. 2. (In Portuguese)
38. Gomes, M.N.; Nascimento, C.D.; Bonafini, B.L.; dos Santos, E.D.; Isoldi, L.A.; Rocha, L.A.O. Two-dimensional geometric optimization of an oscillating water column converter in laboratory scale. *Rev. Eng. Térmica* **2012**, *11*, 30–36. [[CrossRef](#)]
39. Lisboa, R.C.; Teixeira, P.R.; Didier, E. Regular and irregular wave propagation analysis in a flume with numerical beach using a Navier-Stokes based model. *Defect Diffus. Forum* **2017**, *372*, 81–90. [[CrossRef](#)]
40. Gomes, M.N.; Isoldi, L.A.; dos Santos, E.D.; Rocha, L.A.O. Análise de malhas para geração numérica de ondas em tanques. In Proceedings of the Anais do VII do Congresso Nacional de Engenharia Mecânica, Associação Brasileira de Engenharia e Ciências Mecânicas, Rio de Janeiro, Brazil, 31 July–3 August 2012. (In Portuguese)
41. Gomes, M.N.; Lorenzini, G.; Rocha, L.A.O.; dos Santos, E.D.; Isoldi, L.A. Constructal Design Applied to the Geometric Evaluation of an Oscillating Water Column Wave Energy Converter Considering Different Real Scale Wave Periods. *J. Eng. Thermophys.* **2018**, *27*, 173–190. [[CrossRef](#)]
42. Letzow, M.; Lorenzini, G.; Barbosa, D.V.E.; Hubner, R.G.; Rocha, L.A.O.; Gomes, M.N.; Isoldi, L.A.; dos Santos, E.D. Numerical Analysis of the Influence of Geometry on a Large Scale Onshore Oscillating Water Column Device with Associated Seabed Ramp. *Int. J. Des. Nat. Ecodyn.* **2020**, *15*, 873–884. [[CrossRef](#)]
43. Lima, Y.T.B.; Gomes, M.N.; Isoldi, L.A.; dos Santos, E.D.; Lorenzini, G.; Rocha, L.A.O. Geometric Analysis through the Constructal Design of a Sea Wave Energy Converter with Several Coupled Hydropneumatic Chambers Considering the Oscillating Water Column Operating Principle. *Appl. Sci.* **2021**, *11*, 8630. [[CrossRef](#)]
44. Chai, T.; Draxler, R.R. Root mean square error (RMSE) or mean absolute error (MAE)? – Arguments against avoiding RMSE in the literature. *Geosci. Model Dev.* **2014**, *7*, 1247–1250. [[CrossRef](#)]
45. Dizadji, N.; Sajadian, S.E. Modeling and optimization of the chamber of OWC system. *Energy* **2011**, *36*, 2360–2366. [[CrossRef](#)]
46. Holthuijsen, L.H. *Waves in Oceanic and Coastal Waters*; Cambridge University Press: Cambridge, UK, 2007.
47. Strauch, J.C.; Cuchiara, D.C.; Toldo, E.E., Jr.; Almeida, L.E.S.B. O padrão das ondas de verão e outono no litoral sul e norte do Rio Grande do Sul. *Rev. Bras. Recur. Hídricas* **2009**, *14*, 29–37. (In Portuguese) [[CrossRef](#)]

Disclaimer/Publisher’s Note: The statements, opinions and data contained in all publications are solely those of the individual author(s) and contributor(s) and not of MDPI and/or the editor(s). MDPI and/or the editor(s) disclaim responsibility for any injury to people or property resulting from any ideas, methods, instructions or products referred to in the content.